

Motion-induced stresses in pack ice

James K. Lewis

Ocean Physics Research & Development, Long Beach, Mississippi

J. A. Richter-Menge

Cold Regions Research and Engineering Laboratory, Hanover, New Hampshire

Abstract. We consider motion-induced stresses in pack ice through the analyses of a variety of observations collected during the Sea Ice Mechanics Initiative study conducted in the Beaufort Sea during 1993. Motion-induced components of in situ stress from stress gauge data are compared to stresses calculated as residuals based on a force balance argument using observed wind, current, and ice motion data. There is reasonable qualitative and quantitative agreement between the observed and calculated motion-induced stresses in the north-south direction if the residual stress is assumed to be distributed over a horizontal distance of ~ 10 m. To obtain a general agreement with the magnitudes of the observed and calculated stresses in the east-west direction, the residual stress must be considered to be distributed over a horizontal distance of ~ 50 m. There are three significant stress events determined by the force balance calculations, but only the one event in the north-south direction has a strong corresponding signal in the stress gauge data. There is very little indication of the two events in the east-west direction in the gauge data. Numerical simulations of the distribution of motion-induced stresses within a floe show that significant variations in the character of the stresses can occur over short horizontal distances throughout the floe. Hence a seeming lack of a clear correspondence between the observed and calculated stress may be due to our inability to properly recognize the modified signature of the event at the specific locations of the stress gauges. The results suggest that to effectively develop an understanding of the role that point stress measurements can play in developing our understanding of the process of ice deformation, it may be necessary to couple the stress measurements with models of the patterns of motion-induced stresses within a floe. Finally, we consider the relationship between the residual stress and the differential motion of the ice pack as seen by a cluster of drifters on various floes. The three main stress events seen in the residual stresses all occurred during periods of convergence of the floes. However, we have tested various relationships between stress and strain, and they indicate that there should have been additional stress events as a result of other periods of substantial convergences of the ice pack. This suggests the possibility that the residual stresses were not locally generated.

1. Introduction

Basin-scale ice dynamics models are designed to generate dominant sea ice circulation patterns for ice motion of ≥ 100 km [Hibler, 1979; Pritchard, 1988; Preller *et al.*, 1992]. At these scales, the ice cover is assumed to behave as a continuum, and the models typically employ an elastic-plastic or viscoplastic rheology to determine stresses resulting from the differential motion of the ice cover. The specifics of a particular rheology, such as the yield strength of the ice cover, are defined by comparing model-predicted ice motion to the drift of individual ice floes and/or satellite imagery. To address problems that consider smaller, regional-scale ice behavior, it is necessary to increase the resolution of ice dynamics models to the order of 10–25 km. The level of detail provided by higher-resolution models is useful for furnishing navigational guidance and for developing a more complete understanding of the impact of the ice/open water distribution on the thermodynamic interac-

tion of the air, ice cover, and ocean. Higher-resolution models are also important for establishing the impact of scale on the mechanical behavior of the ice cover and for studying sea ice behavior near coastal boundaries.

Investigations have been made that consider the application of basin-scale models at the regional scale. These efforts have met with limited success [Tucker, 1982; Overland and Pease, 1988; Preller *et al.*, 1990]. Typically, it has been necessary to modify the ice rheology to achieve a reasonable agreement between model-predicted and observed ice motion at the smaller spatial scales of regional models. Such a necessity is consistent with the observations made by Overland *et al.* [1995] which indicate that the mechanical behavior of the ice cover should be considered as a hierarchical system with natural divisions of scale. Overland *et al.* [1995] suggest that there exist scale divisions between the 100- to 300-km scale, the 10- to 50-km scale, and the 1-km scale for the mechanical behavior of an ice cover. At the 100- to 300-km scale, the processes governing sea ice motion can be resolved by considering the aggregate behavior of the ice cover. At the 10- to 50-km scale, Overland *et al.* [1995] found it necessary to resolve shearing behavior. This apparent change in the mechanical behavior of

Copyright 1998 by the American Geophysical Union.

Paper number 98JC01262.
0148-0227/98/98JC-01262\$09.00

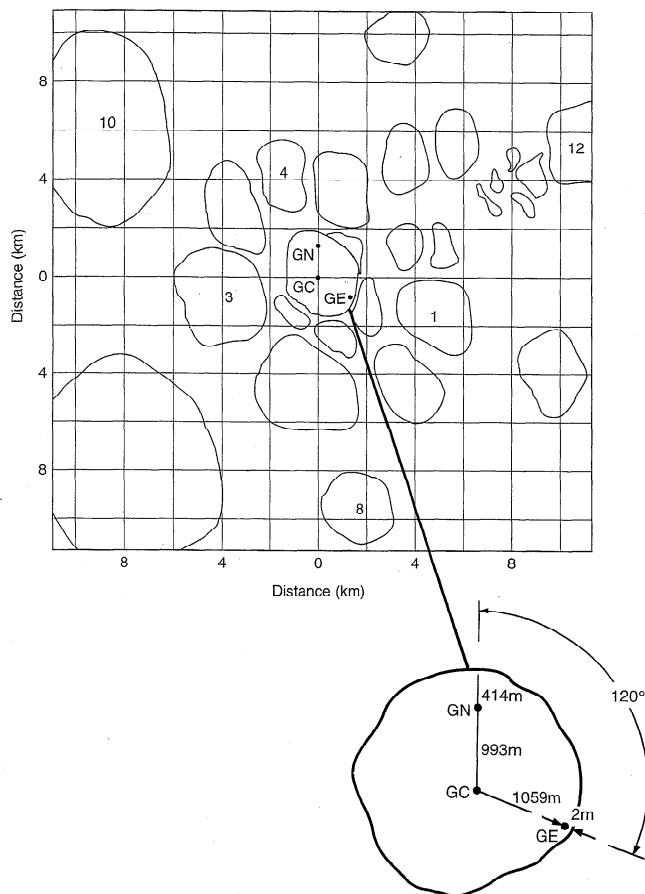


Figure 1. Initial positions of the Sea Ice Mechanics Initiative (SIMI) main floe (location (0, 0)) and surrounding floes (labeled with numbers) whose positions were used to calculate differential motion about the main floe. At the beginning of the experiment, the main floe, with a diameter of 3 km, was located at 75°N, 142°W. Also shown are the locations of stress gauges GC, GN, and GE. This represents a portion of the stress and deformation array installed for SIMI, through a cooperative effort between Cold Regions Research and Engineering Laboratory (CRREL) and Pacific Marine Environmental Laboratory, National Oceanic and Atmospheric Administration (NOAA). This map is a cartoon produced by J. Overland (NOAA) and J. Richter-Menge (CRREL) after a number of consecutive helicopter survey flights over the area. There is less detail in the location of adjacent floes with distance from the central floe.

the ice cover may also be related to the granular nature of the ice cover, where the “grains” are the individual floes. *Guterl* [1996] describes work being done to develop a more thorough understanding of the properties of sand. These studies indicate that because the granularity of sand is readily apparent at the human scale, the movement of sand as it flows cannot be modeled as a fluid. Instead, the interaction of the individual particles must be addressed to develop an accurate prediction of the flow process. The same may be true for the ice pack at scales of 10 to 25 km where, if one were to apply a granular model, a floe would be considered the basic element.

To directly assess the mechanical behavior of the Arctic pack ice at regional scales, the Office of Naval Research initiated a program of concurrent measurements of in situ ice stresses and ice motion called the Sea Ice Mechanics Initiative (SIMI). A

stress and deformation array was established over a 20-km region of the pack ice in the Alaskan Beaufort Sea, and measurements were recorded over 6 months, beginning in September 1993. Early comparison of the measurements indicated that there was a correspondence between stress and ice motion [*Richter-Menge et al.*, 1996]. The correspondence became more pronounced as the area of deformation being considered in the comparison was increased.

In this paper, we take a step toward developing a more detailed understanding of the relationship between observed stresses and ice pack deformation during SIMI by focusing on the characteristics of the motion-induced stresses in floes. Since stresses in a floe result from both thermal as well as motion-induced processes, the first part of our paper describes work dealing with estimating those stresses due strictly to ice motion. With a satisfactory estimate of the motion-induced stresses in hand, we use a number of techniques to develop an understanding of how these stresses are generated. These techniques include a comparison of the measured stresses to those stresses determined as residuals from a force balance analysis using SIMI wind, under-ice current, and ice motion data. The characteristics of the stresses determined from the force balance analysis are described as they relate to the observed motion-induced stresses and the differential motion of the floes in the SIMI region. Finally, numerical simulations are used to investigate the complex distribution of motion-induced stress within a multiyear floe. The results of the simulations clearly show the complexity and limitations of assessing motion-induced stresses based on stress measurements made at a few locations in a floe and without specific knowledge of the forcing all along the edges of the floe.

2. Observations

2.1. Ice Motion, Winds, and Currents

During September 1993, a 20-km region in the Alaskan Beaufort Sea at ~75°N and 142°W was instrumented with 13 Argos buoys, all on different floes. One buoy was put on the floe with the main SIMI camp, while the others were placed in two circles at ~5- and 10-km radii about the main camp floe. Of these 13 tagged floes, Global Positioning System (GPS) position data from seven were used in this study of motion-induced stresses in the floe with the main SIMI camp, and these are depicted in Figure 1. In addition to the floe drift data, wind velocity, stress gauge, and under-ice current data relative to the main SIMI floe were available. Finally, ice core observations during SIMI were used to determine estimates of the average temperature and porosity of the main SIMI floe, which had an average thickness of 1.42 m and a diameter of ~3 km.

On the basis of the coverage of various data sets, this study concentrated on the 1993 period of the SIMI experiment. Specifically, we studied the relationships between ice motion, forcing by winds and ocean currents, and observed stresses during Julian days 340 through 365, 1993. Prior to Julian day 330, the stress observations showed that the stress components σ_x and σ_y at each stress gauge had nearly the same values at all times, where σ_x is the compressive (positive)/tensile (negative) stress component in the east-west (x) direction and σ_y is the compressive/tensile stress in the north-south (y) direction. Moreover, the stresses at all three locations on the main SIMI floe (Figure 1) were nearly identical. Correlation analyses of the ice stress and temperature indicate that thermal processes dominated the stressing of the floe prior to day 330 [*Richter-Menge*

and Elder, this issue]. It was only after day 330 that the σ_x and σ_y stresses at each gauge began to take on different values and significant differences between individual gauges existed. Since under-ice current observations were begun only on day 337, we concentrated on the 25-day period between days 340 and 365.

The movement of the ice pack for days 340–365 was primarily westward, with a slight southward component. Figure 2 shows the velocity (u , v) of the main ice camp (u being east, v being north) corresponding to the observed wind velocity (U , V) (U being east, V being north). It is quite clear that the movement of the ice pack was principally a result of wind forcing. In general, the changes in wind velocity precede changes in ice velocity. An exception to this tendency is when the ice began to move northward during days 359–362 while the wind remained mostly westward.

Also shown in Figure 2 are the ocean currents relative to the ice velocity of the main SIMI floe. These current data were collected at a site near the center of the SIMI floe at 3.4 m below the bottom of the ice. The relative ocean currents are almost an exact mirror image of the ice velocity, implying the extraction of momentum from the ice by the ocean.

The drift data from seven of the Argos-tagged floes were used to calculate differential motion of the floes in terms of the strain rates $\epsilon_{xx} = \partial u/\partial x$, $\epsilon_{yy} = \partial v/\partial y$, and $\epsilon_{xy} = \partial u/\partial y + \partial v/\partial x$. The method for calculating these kinematic parameters is described by Lewis and Giuffrida [1989]. The rms error for the position data is estimated to be ~ 30 m, and the bias in the kinematic parameters resulting from the rms position error was minimized following Kirwan and Chang [1979]. The ϵ_{xx} and ϵ_{yy} strain rates are shown in Figure 3. The strain rates in the north-south direction are seen to be an order of magnitude smaller than those in the east-west direction. Positive strain rate values tend to relieve any compression in the ice pack, but

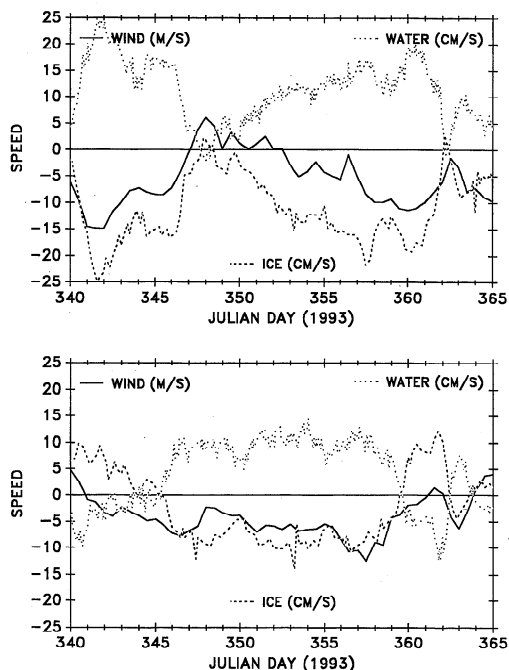


Figure 2. Observed speeds of the main SIMI floe (u , v) and corresponding wind speed (U , V) and relative water speed (u_o , v_o) for (top) the east-west components (positive being east) and (bottom) the north-south components (positive being north).

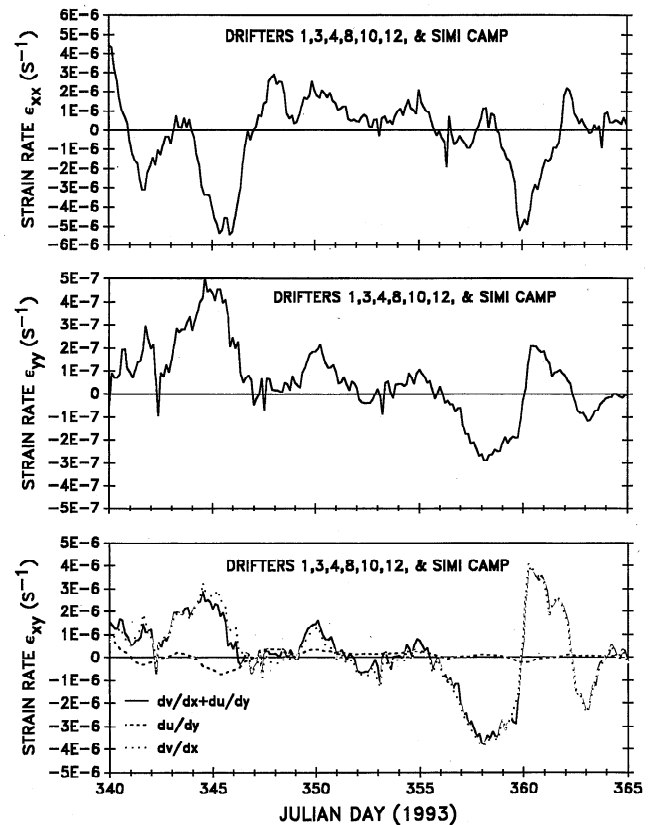


Figure 3. Calculated ϵ_{xx} , ϵ_{yy} , and ϵ_{xy} strain rates based on observed floe motion. Positive (negative) ϵ_{xx} and ϵ_{yy} strain rates tend to produce tensile (compressive) stresses.

we do not believe positive strain rates would ever produce tensile stresses in a floe because of the relatively weak linkages between adjacent floes. Negative strain rates tend to produce compressive forces in the ice pack, but only if the ice pack is compact enough to result in floe-floe interactions.

The shearing strain rate ϵ_{xy} is also shown in Figure 3, along with its two components, $\partial u/\partial y$ and $\partial v/\partial x$. The shearing strain rate is of the same order as the compressive/tensile strain rate ϵ_{xx} , $\sim 10^{-6} \text{ s}^{-1}$. However, the major component is $\partial v/\partial x$, with $\partial u/\partial y$ being up to an order of magnitude smaller. Once again, the shearing strain will produce stresses within floes only if the ice pack is compact enough to result in floe-floe interactions.

The change in the orientation of the cluster of tagged floes was determined by the calculated vorticity. The vorticity is also of the order of 10^{-6} s^{-1} (a little less than 5° per day), and there was some significant changes in the orientation of the cluster of floes with time. Figure 4 shows the calculated direction clockwise from north of the edge of the main SIMI floe that was originally pointing north. At day 340, that edge would have been orientated toward the northeast, but it rotated back and was pointing approximately northward from days 345 to 357. It then rotated back to the northeast.

2.2. Ice Stresses at the Main SIMI Floe

A total of 26 stress sensors were placed in the 3-km-diameter main SIMI floe in an array designed to measure the spatial variability of stress in a multiyear floe. These sensors were distributed among three sites near the edge and a site at the

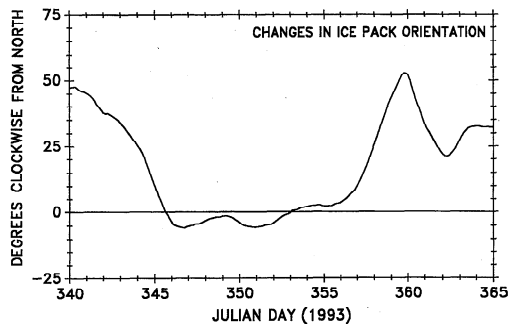


Figure 4. Calculated variations in the orientation of the ice pack (clockwise from north) based on observed floe motion.

center of the floe. Details of the sensor locations relative to the boundary of the floe and ice cover surface are provided by *Richter-Menge and Elder* [this issue]. Briefly, most of the sensors were located near the surface of the ice, at constant depth relative to the water surface. The depth of the sensors varied from 20 to 44 cm below the ice surface and was dependent on the ice freeboard at the time of installation. The sensors used in the study were the cylindrical, vibrating wire sensors described by *Johnson and Cox* [1982]. They provide a point measurement of stress. Extensive laboratory tests under controlled loading conditions indicated that over a loading range of 1 to 2 MPa, the measured stress was within 15% of the applied stress and the stress direction was typically correct to within 5° [*Cox and Johnson*, 1983]. Calibration of each stress sensor establishes a zero-stress datum that is accurate to ± 20 kPa. In addition to ice stress, the ice temperature at the sensor is determined by a thermistor installed in the sensor. Detailed measurements of the temperature profile of the ice cover at the center of the main floe were also made using a thermistor string that extended above and below the ice surface [*Perovich et al.*, 1997].

In this study we concentrated on the data from three particular gauges (Figure 1, inset). These gauges were chosen because of their relative location in the floe. The first gauge (referred to as GC) was located at about the center of the nearly circular, 3-km floe. The second gauge (referred to as GN) was located toward the edge of the floe that was originally pointing toward the north, ~ 1100 m from the center of the floe and 400 m from the edge of the floe. The third gauge (referred to as GE) was located on the edge of the floe that was originally pointing just south of east, ~ 2 m from the ice edge. Stresses at the GC, GN, and GE sites were measured at depths of 38, 20, and 44 cm below the ice surface, respectively. Combined, these stress records indicate the extreme spatial variability of stresses in the floe, which is a function of the boundary conditions and stress attenuation.

The stress observations [*Richter-Menge and Elder*, this issue] were converted to compressive/tensile stresses in the east-west and north-south directions after accounting for the changing orientation of the floe (Figure 4). The data from GC are shown in Figure 5. The compressive/tensile stresses in the east-west direction (referred to as σ_{xC}) varied relatively slowly over the 25-day period, going from compressive stresses from days 340–347 to tensile stresses during days 348–362 then back to compressive stresses. Compressive stresses were ~ 25 kPa, while the tensile stresses were as large as ~ 75 kPa. The compressive/tensile stresses in the north-south direction (referred to as

σ_{yC}) followed the general variations of σ_{xC} almost exactly, but with an offset of $\sim +12$ kPa (more compressive).

The stress data for days 340–365 from GN are also shown in Figure 5. There are distinct north-south compressive events in

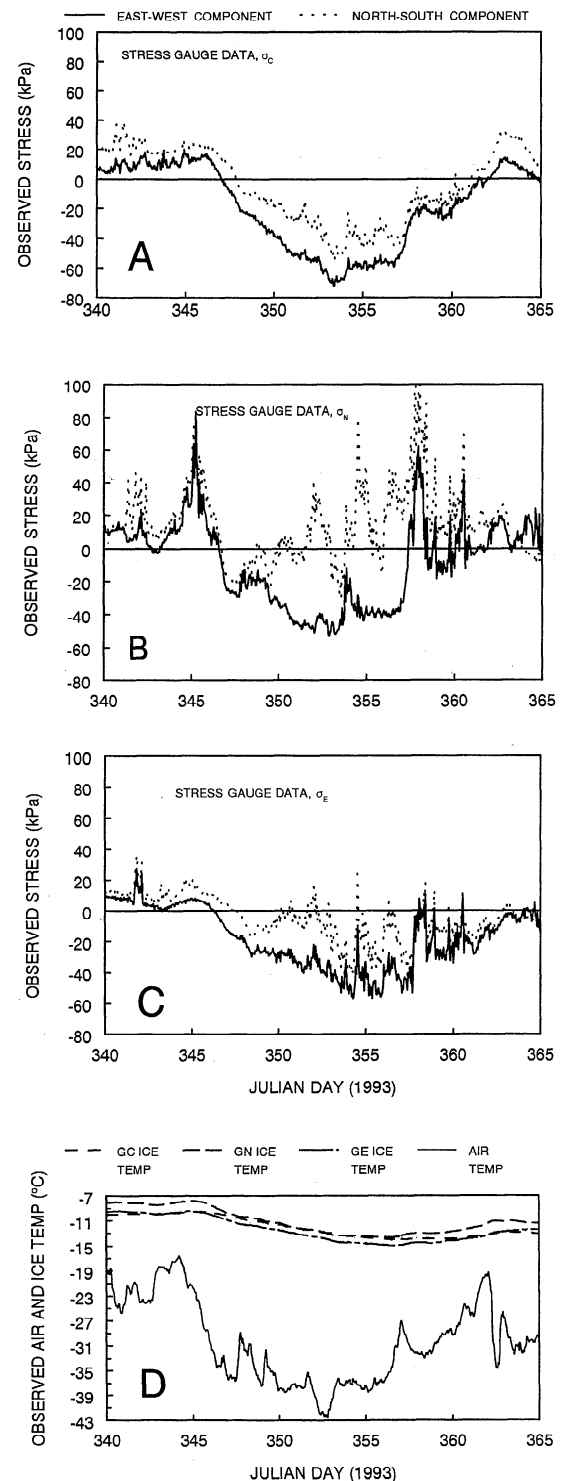


Figure 5. Compressive (positive)/tensile (negative) stresses (a) observed at the center of the main SIMI floe, (b) near the edge of the main SIMI floe that was originally pointing toward the north, and (c) near the edge of the main SIMI floe that was originally pointing toward the east and (d) air temperature data as well as ice temperature data at each stress gauge.

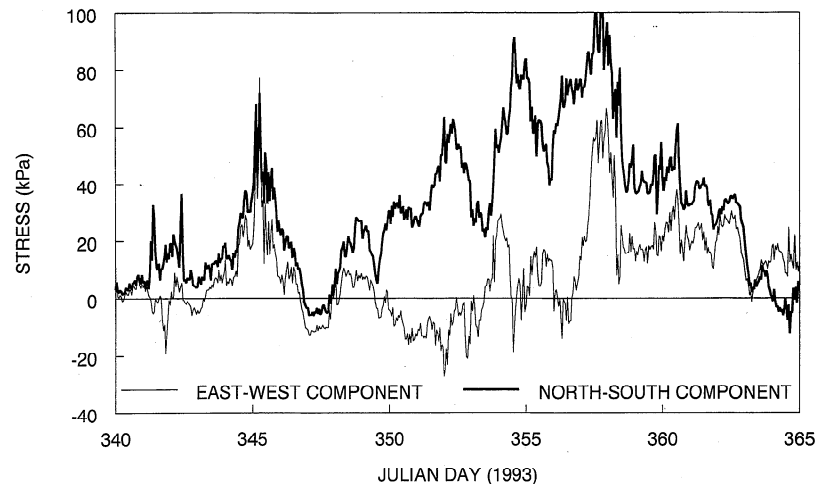


Figure 6. Estimates of the motion-induced stress components σ'_{xN} and σ'_{yN} near the edge of the main SIMI floe that was originally pointing toward the north.

the data (referred to as σ_{yN}), some reaching 75 kPa and larger. The compressive/tensile stresses in the east-west direction at GN (referred to as σ_{xN}) also have some compressive events, the more significant ones corresponding to those in the north-south direction.

Figure 5 also shows the stress data from GE. The east-west component of GE (referred to as σ_{xE}) is similar to the east-west components of GN and GC, except for the compression events seen in GN. In fact, it is of interest to note that there are very few periods of compression in either the east-west or north-south (referred to as σ_{yE}) components of GE, even though ϵ_{xx} was an order of magnitude larger than ϵ_{yy} .

Thermal processes are responsible for some of the stress variations seen in the data [Richter-Menge and Elder, this issue], and an attempt was made to eliminate the thermally induced stresses. Unfortunately, there is no definitive way of discerning just the thermal component of the stress observations from the data we have on the SIMI floe. Thermally induced strain rates throughout the floe impact the strain rates at a given point since such floes are too big to bend or twist in response to spatial variations of strain rates [Lewis, 1994a, b]. As such, to determine thermally induced stresses, we must have data on the spatial and temporal variations of the snow cover, a key piece of data that was not collected during SIMI. As an alternative, a variety of methods were explored to approximate the thermally induced stresses. During the Arctic fall, thermally induced stresses result from the passages of warm and cold fronts [Lewis, 1994b] and therefore can correspond in time (and, in many cases, magnitude) with motion-induced stress variations. Therefore we cannot always eliminate thermally induced stresses by the band-pass filtering of the observed stresses. Richter-Menge and Elder [this issue] developed a scheme to eliminate thermal stresses based on the fact that the minor principal stress component was correlated with ice temperature at all the stress gauges at a level of 0.75 to 0.91. Thus, in their scheme, estimates of motion-induced stresses were obtained by subtracting the minor principal stress component from the major principal stress component and converting to an east-west/north-south coordinate system.

Here we try another tack for estimating the thermal stresses in the observations based on the results of the modeling of compressive stresses within a floe by Frederking and Evgin

[1990]. The results of their study indicate that a compressive stress applied in the x direction across a circular floe will result in compressive stresses in both the x and y directions near the two edges of the floe across which the stress is being applied. At the other edges of the floe ($\pm 90^\circ$ along the circular floe), the applied compressive stress results in a reduced compressive stress in the x direction and a small tensile stress in the y direction that goes to zero right at the edges of the floe. In other words, the application of any east-west or north-south compressive loading will never result in any significant tensile stresses near the edges of the floe.

Considering these results (and neglecting the impact of shearing stresses applied along the edges of the floe, which will be addressed later), then σ_{xE} and $\sigma_{yE} < 0$ would likely be thermally induced. For $\sigma_{xE} > 0$, the stress could be transmitted to GN, according to Frederking and Evgin [1990], but at a substantially reduced magnitude. However, if we compare the observations, $\sigma_{xE} > 0$ is reproduced almost exactly by σ_{xN} and σ_{yN} , and in any cases, the corresponding stresses at GN are greater than σ_{xE} .

These results seem to imply that σ_{xE} is primarily a result of thermal stresses, not motion-induced stresses. If this is the case, then $\sigma'_{xN} = \sigma_{xN} - \sigma_{xE}$ and $\sigma'_{yN} = \sigma_{yN} - \sigma_{xE}$ provide estimates of the motion-induced stresses at GN plus any residual thermal component not seen at GE. The σ'_{xN} and σ'_{yN} stress components are shown in Figure 6. There are significant σ'_{yN} compressive events during almost the entire period, along with some corresponding σ'_{xN} compressive events. Although these estimates of motion-induced stresses are based on the highly idealized and simplified modeling results of Frederking and Evgin [1990], the estimates are quite similar to those determined by Richter-Menge and Elder [this issue].

Another means for estimating nonthermal stresses can be performed based on the facts that (1) the governing equations used by Frederking and Evgin [1990] did not include the viscous creep of the ice and (2) at the rates at which the pack ice was being strained (Figure 3), creep can have a significant impact on the magnitude of stresses within the floe. The results of Frederking and Evgin [1990] imply that stresses at the center of a floe are reduced from their magnitudes at the edge of the floe as a result of shearing stresses. In effect, the stress is redistributed laterally across the floe by shearing motion, and an atten-

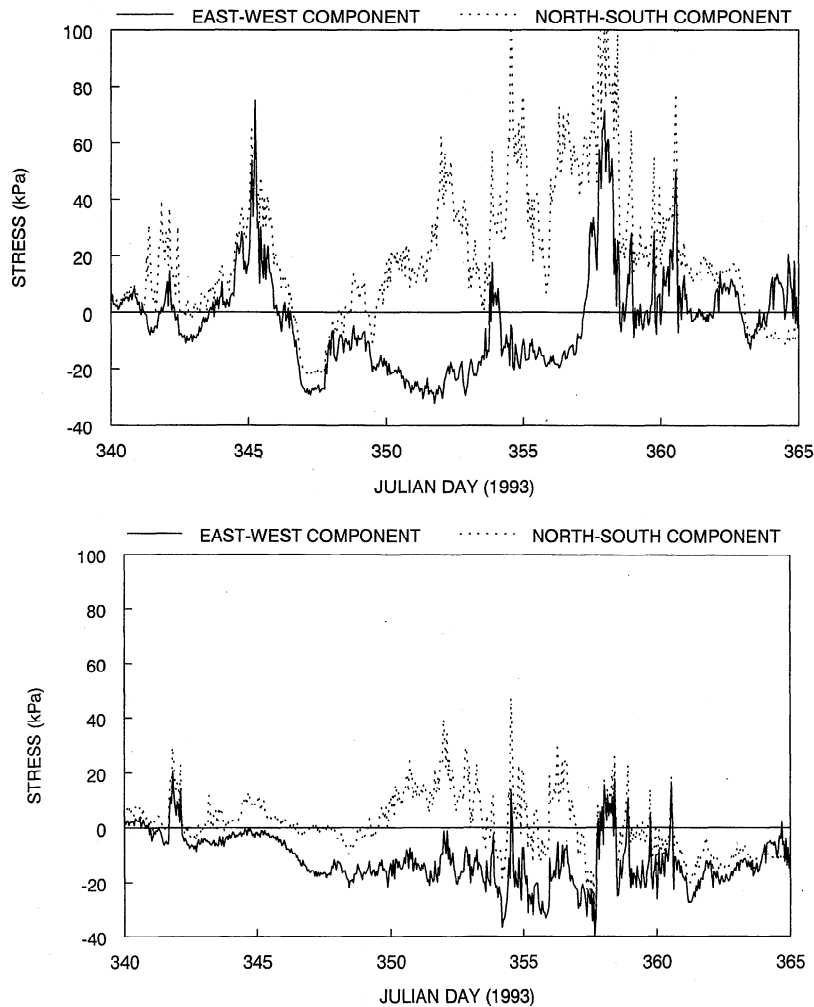


Figure 7. Estimates of the motion-induced stress components at (top) GN and (bottom) GE. These estimates were obtained by subtracting $(\sigma_{x_C} + \sigma_{y_C})/4$ from the observed stresses.

uation of the stress magnitude is seen moving toward the center of the floe. This reduction in stress magnitude has been observed in stress measurements across a floe [Perovich *et al.*, 1992] and, according to the results of Frederking and Evgin [1990], can be up to 80%; but creep always tends to decrease the magnitude of the stress in ice (whether tensile or compressive), so we might expect the reduction in magnitude to be even greater than that indicated by Frederking and Evgin [1990]. Thus the stresses measured at GC at the center of the SIMI floe may be a good estimate of thermally induced stress with a minimal influence of motion-induced stress. In particular, the average of σ_{x_C} and σ_{y_C} may provide a reasonable approximation to thermally induced stresses. We estimated the motion-induced stresses at GN and GE (plus any residual thermal component not seen at GC) by subtracting $(\sigma_{x_C} + \sigma_{y_C})/2$ from the observed stresses. The estimated stresses at GN using this method (not shown) are quite similar in magnitude and variation as the estimates shown in Figure 6. The estimated motion-induced stresses at GE (not shown) indicate a somewhat different stress regime than that at GN. To a large degree, we found that both stress components at GE are mirror images of the mean stress at the center of the floe, which might imply that $(\sigma_{x_C} + \sigma_{y_C})/2$ is an overestimate of the thermally induced stresses for GE (if there were a few more centimeters

of snow cover at GE relative to the center, thermally induced stress variations could be significantly less in magnitude). In fact, when we subtract only 50% of $(\sigma_{x_C} + \sigma_{y_C})/2$ from the observed stresses at GE, the resulting stresses (our estimates of the motion-induced stresses) become relatively small. This would again imply that most of the stress variations along the GE edge of the SIMI floe are thermally induced.

Here we use $(\sigma_{x_C} + \sigma_{y_C})/4$ as our best estimate for the thermally induced stresses at both GN and GE. The estimates of the motion-induced stresses at GN and GE based on this approach are shown in Figure 7. Again, these estimates are quite similar to those made by Richter-Menge and Elder [this issue], except that there are periods during which the ice is in tension, while Richter-Menge and Elder's technique never produced tensile stresses (the generation of motion-induced tensile stresses is discussed in section 4). The estimates of Richter-Menge and Elder [this issue] are based on fairly strong correlations between the variations of the minor component of the principal stress vector and changes of the ice temperature, of the order of 0.85 for the time considered in our study. Thus the ability of using $(\sigma_{x_C} + \sigma_{y_C})/4$ to produce motion-induced stresses that are quite similar to those of Richter-Menge and Elder provides a high level of confidence in our technique.

3. Motion-Induced Stresses

There are several methods with which we can indirectly estimate motion-induced stresses in the main SIMI floe. One means is to use the force balance equations for a floe and calculate the residual stress that results in a balance of the various terms in the momentum equations. These residuals should correspond to nonthermally induced stresses observed in GN and GE. To perform such calculations, we use the velocity and position data of the main SIMI floe, the observed wind forcing, and estimates of the drag of the ocean on the bottom of the floe. We ignore sea surface tilt.

The force balance governing equation is

$$H\rho[D\mathbf{u}/Dt + f\mathbf{k} \times \mathbf{u}] = \tau_s - \tau_b + \mathbf{S} \quad (1)$$

where $\mathbf{u} = (u, v)$, t is time, D/Dt is the total derivative with respect to time, f is the Coriolis parameter, \mathbf{k} is the unit vertical vector, τ_s is the surface wind stress vector, τ_b is the bottom ocean current stress vector, \mathbf{S} is the residual stress, H is the mean thickness of the floe (1.42 m for the SIMI floe), and ρ is the ice density (917 kg/m³). The position data are used to calculate the left-hand side of the above expression. Wind, ice, and current velocity data are used to calculate the right-hand side, allowing \mathbf{S} to be determined as a residual. The values of \mathbf{S} represent means over the volume of the floe, so we can only expect a qualitative agreement between the calculated \mathbf{S} and our estimates of the motion-induced stresses at GN or GE.

Wind stress is calculated using $\tau_s = \rho_{\text{air}} C_{10} \mathbf{W}|\mathbf{W}|$, where $\rho_{\text{air}} = 1.395 \text{ kg/m}^3$, $\mathbf{W} = (U, V)$, $|\mathbf{W}| = (U^2 + V^2)^{1/2}$, and $C_{10} = 1.04 \times 10^{-3} + 1.21 \times 10^{-3}/(1 + e^{-(|\mathbf{W}|-12.5)/1.56})$ [Amorocho and DeVries, 1981]. Bottom stress is calculated using $\tau_b = -\rho_w C_D \mathbf{U}_o |\mathbf{U}_o|$, where $\rho_w = 1025 \text{ kg/m}^3$, $\mathbf{U}_o = (u_o, v_o)$ is the measured relative ocean current, and $C_D =$

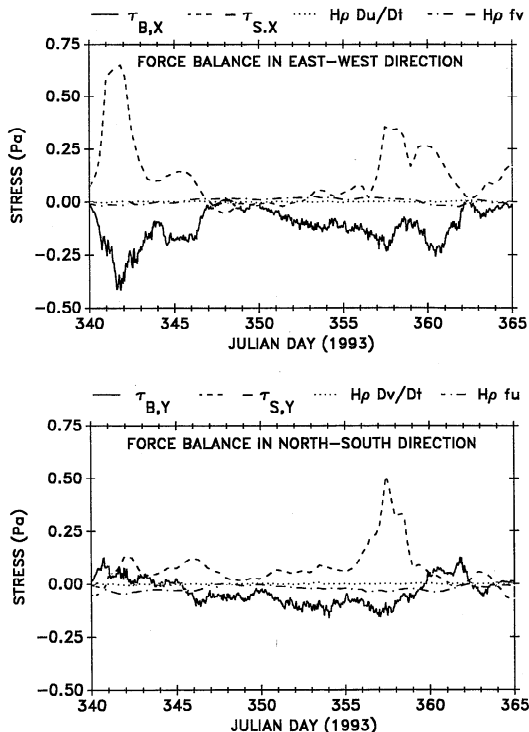


Figure 8. Calculated components of the momentum balance equation (1) in the (top) east-west and (bottom) north-south direction.

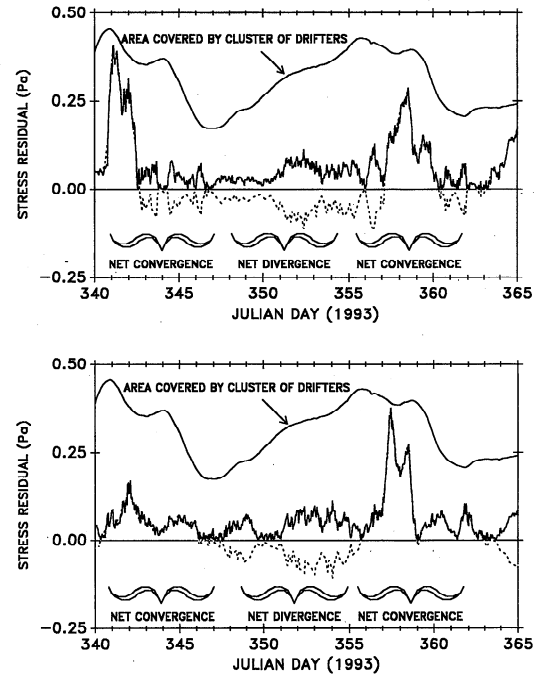


Figure 9. Residual stresses determined using (1) in the (top) east-west direction (S_x) and (bottom) north-south direction (S_y). The dashed lines are the calculated residuals, while the solid lines are the absolute values of the residuals. Also shown are the time variations of the relative area covered by the drifters on the ice.

6.07×10^{-3} based on a roughness of $\sim 2 \text{ cm}$ [Lewis, 1994a]. The negative sign in the expression for τ_b is a result of the ocean currents already being relative to the ice velocity.

The variations of the different components in (1) are shown in Figure 8. The inertia and Coriolis terms tend to be small, resulting in a balance primarily between wind stress and under-ice water stress. The residual stress \mathbf{S} is calculated as the sum of the other four terms, and the variations of \mathbf{S} are shown in Figure 9, along with $|\mathbf{S}|$. In general, we see that east-west residual stress S_x is westward in direction, except for days 340–342.5, 357.5–360, and 363–365. However, these eastward directed residual stresses tend to be the more significant in magnitude than the westward directed residual stress. The north-south residual stress S_y is mostly northward in direction. The larger S_y magnitudes tend to occur at the same times as those of S_x .

The residual stresses shown in Figure 9 indicate that there were two major residual stress events in S_x . The first occurred mostly during day 341, and the second occurred over the period of days 357–360. The results in Figure 9 also show that there was only one major residual stress event in S_y , and this occurred during days 356–359. Also shown in Figure 9 is the relative area covered by the cluster of drifters. This area is the time-integrated divergence $D(\partial u/\partial x + \partial v/\partial y)$, assuming an initial area of 1.0 on day 268. It can be seen that the first residual stress event in S_x occurred during a period of convergence. The second S_x event occurred during overall convergence but reached its peak during a period of divergence. As for the residual stress event in S_y , it reaches its peak during a period of convergence, but it also reaches a secondary peak in stress during a period of divergence. Both the second S_x event and the S_y event occur after a period of overall divergence that

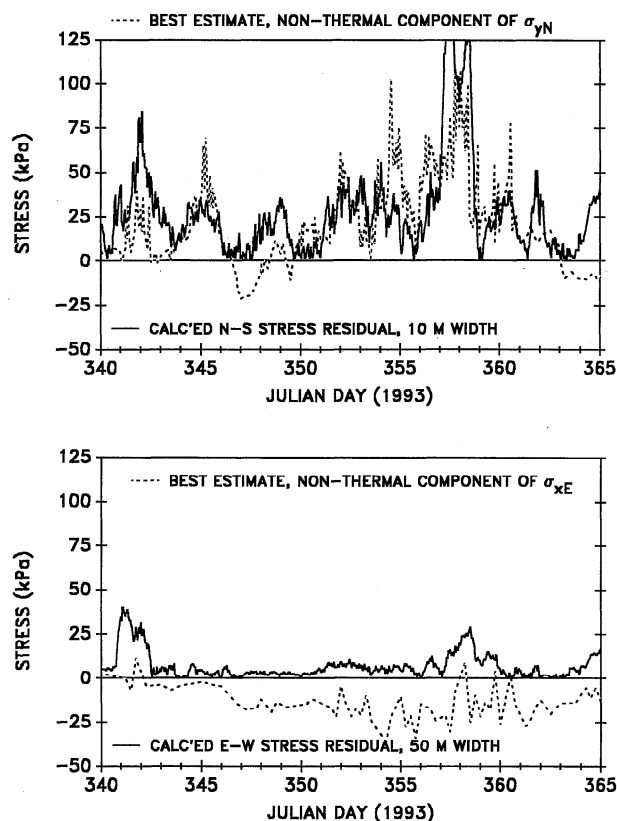


Figure 10. Comparisons between the calculated residual stress $|S_x|$ and (top) σ_{yN} based on a 10-m Δx and (bottom) σ_{xE} based on a 50-m Δy .

took place from days 346.5 to 355.5. These are rather curious relationships between residual stress and the divergence/convergence of the ice in the study area; but an even more peculiar situation is that there are no residual stress events for the periods of major convergence for the ice, the first during days 344–347 and the second during days 359–362. During both of these periods, the relative area was reduced by ~50%. Yet there are no dramatic increases of the residual stresses during the times of these convergences.

If the residual stresses calculated by the force balance argument and the nonthermal gauge observations are both a manifestation of the same stress field (a product of whatever is happening at the boundaries), we could expect some relationship between the sets of stresses. The residual stress is in terms of force per unit horizontal area. To make a comparison between the calculated residual stress and the stress gauge data, we convert the residual to force per unit vertical area by multiplying by the area of the floe (approximately $\pi \times 1500^2 \text{ m}^2$) and then dividing by the thickness of the ice (1.42 m) times the width over which the force is applied (Δx). For example, for a residual stress of 0.2 Pa, the stress felt over a 1000-m width Δx would be 1.0 kPa. Figure 10 shows the variations of our best estimate of the nonthermal component of σ_{yN} and $|S_y|$ in terms of a Δx of 10 m. We see that there is both a quantitative as well as a qualitative agreement between the observed and calculated stresses based on a 10-m Δx . As for the residual stress in the east-west direction, the fact that we have concluded that thermal stresses dominated the observed σ_{xE} would imply that the Δy over which S_x was distributed was

larger than 10 m. Shown in Figure 10 is our best estimate of the nonthermal component of σ_{xE} , along with $|S_x|$ in terms of a Δy of 50 m. The distribution over a greater area does not lessen the importance of S_x in terms of a balance of forces, but it does minimize its signature at a stress gauge relative to thermally induced stresses or other minor motion-induced forces that are acting over a smaller Δy .

Although matching the residual stresses to the motion-induced gauge stresses can be made logically in terms of horizontal scales over which the forces are distributed, this may, in fact, be an oversimplification of the problem. The scales Δx and Δy can also reflect deviations of the locations at which the gauge data were collected relative to the forcing at the boundaries of the floe. This is investigated in the section 4.

4. Simulations of Motion-Induced Stresses in a Floe

4.1. Governing Equations

The stress state at a given location within a floe is governed by the conservation of momentum and versions of Hooke's law. The momentum equations are of the form

$$\partial u_i / \partial t + \partial(u_i u_i) / \partial x + \partial(u_i v_i) / \partial y = [\partial \sigma_{xx} / \partial x + \partial \sigma_{sx} / \partial y] / H \rho \quad (2)$$

$$\partial v_i / \partial t + \partial(v_i u_i) / \partial x + \partial(v_i v_i) / \partial y = [\partial \sigma_{yy} / \partial y + \partial \sigma_{sy} / \partial x] / H \rho$$

where (u_i, v_i) are the vertically integrated velocities within the ice floe in the x (east) and y (north) directions, respectively; t is time, σ_{xx} is the tensile/compressive stress component in the x direction; σ_{sx} is the shearing stress component in the x direction; σ_{yy} is the tensile/compressive stress component in the y direction; and σ_{sy} is the shearing stress component in the y direction. Again, H is the thickness of the ice, and ρ is the ice density. We assume that the ice within the floe is irrotational, giving $\sigma_{sx} = \sigma_{sy} = \sigma_s$.

In terms of tensile/compressive stresses, an appropriate rheological law for motion-induced strain rates is a Maxwell viscoelastic relationship of the form

$$\begin{aligned} \partial \sigma_{xx} / \partial t &= E'_x [\epsilon_{xx} - \gamma_x] / [1 - \nu^2] \\ \partial \sigma_{yy} / \partial t &= E'_y [\epsilon_{yy} - \gamma_y] / [1 - \nu^2] \end{aligned} \quad (3)$$

where E'_x and E'_y are effective elastic moduli in the x and y directions, respectively, ν is the Poisson ratio, and γ_x and γ_y are the viscous creep rates of the ice in the x and y directions, respectively. The effective elastic modulus varies with the temperature, strain rate, and porosity of the ice. Creep is included here for completeness since the strain rates shown in Figure 2 and 3 are of the order such that the viscous give of the ice under stress can have an important impact over time [Lewis, 1994a]. Creep varies with the temperature, porosity, and magnitude of the stress of the ice.

In terms of shearing stresses, the governing equation is of the form

$$\partial \sigma_s / \partial t = G [\epsilon_{xy} - \gamma_s] \quad (4)$$

where G is the shearing modulus of the ice and γ_s is the creep associated with shearing stress. Equations (2) through (4), along with appropriate boundary conditions, can be solved numerically to determine the stress state within a floe covered by a grid. We use finite difference approximations to (2)–(4), centered in space and time, to determine the velocity and stress

fields within the numerical grid. We use a numerical grid that can have varying dimensions of individual grid cells within the floe. The u_i velocity is on the right-hand side of each grid cell, the v_i velocity is on the bottom of each grid cell, σ_{xx} and σ_{yy} are defined in the center of each grid cell, and σ_s is defined at the bottom left-hand corner of each grid cell.

Besides defining ε_{xx} , ε_{yy} , and ε_{xy} along the open boundaries, we must also specify E' , G , and γ within each grid cell. Following Lewis [1994a, this issue], the effective elastic modulus is defined by

$$E'(T, P, \text{STR}) = [\varpi \log(\text{STR} + 3) + 3.5 \text{ GPa} (1 - 7.5472 P)(1 - 0.0714 T)]$$

where T is the ice temperature at a given time, P is ice porosity, $\text{STR} = |\varepsilon - \gamma|$ is the overall strain rate for the given time, and $\varpi = 0.1 \text{ GPa}/\log(\text{STR})$. The temperature T reflects the mean temperature through the floe. In these simulations, we use $T = -4.0^\circ\text{C}$. The porosity P used is the average porosity from all the ice cores taken at the main SIMI ice floe; $P = 0.1258$. On the basis of Mellor [1986], the Poisson ratio is determined by

$$\nu = 0.5 - E'/(9 \times 10^9 \times 6).$$

The shearing modulus is then defined as $G = E'/[2(1 + \nu)]$.

We have included creep for completeness, but its impact is secondary and primarily important for accurately determining the stress state for forcing over time (order of a day and longer). The formulation used for creep is

$$\gamma = 1.86 \times 10^{-15} (1 - T)^{-5.25} [\sigma/(1 - P^{1/2})^2]^n + 3.63 \times 10^{-29} (1 - T)^{-2.09} [\sigma/(1 - P^{1/2})^2]^4$$

where the units are s^{-1} , σ is the stress in pascals, and n has a value of $1.36(1 - T)^{0.19}$ [Lewis, 1994a, this issue]. Since the computations presented here do not involve forcing over long periods of time, we do not believe creep plays a significant role in determining the resulting stress fields.

4.2. Boundary Conditions

Boundary conditions are specified for each grid cell that defines the outside edges of the floe. The boundaries are at the u_i or v_i legs of the grid cells. If no strain rate forcing is defined for a given grid cell, then the model calculates the velocity component on the boundary leg of the boundary grid cell using (2) with a zero stress directly outside of the grid cell (that is, $\sigma_{xx} = \sigma_{yy} = \sigma_s = 0$). This allows stress relief through the nonstrained edges of the floe. For those outside edge grid cells for which a strain rate is specified (i.e., ε_{xx} or ε_{yy} nonzero), the velocity component u_i or v_i on the boundary leg of the grid cell is calculated using $u_i = u_{im} \pm \varepsilon_{xx} \Delta x$ or $v_i = v_{im} \pm \varepsilon_{yy} \Delta y$, where (u_{im}, v_{im}) are the velocity components of the next interior grid cell; ε_{xx} and ε_{yy} are the specified strain rates at the boundaries; Δx and Δy are the grid spacing at the boundaries in the x and y directions, respectively; and the plus sign is used for the right-hand side and top boundaries and the minus sign is used for the left-hand side and bottom boundaries.

For those situations in which a shearing stress is defined at a boundary ($\partial v/\partial x$ or $\partial u/\partial y$), the appropriate velocities on the inside edges of the boundary grid cells are calculated using $u_i = u_{im} \pm \Delta y \partial u/\partial y$ or $v_i = v_{im} \pm \Delta x \partial v/\partial x$.

4.3. Simulation Results

We present here the results of two simulations of a nearly circular floe with dimensions of the main SIMI floe ($\sim 3000 \text{ m}$ in diameter). The first simulation was with a compressive forcing in the x direction, and the second was with a shearing forcing $\partial v/\partial x$. The magnitude of each forcing was a strain rate of 10^{-6} s^{-1} . Even though the simulations included the entire dimensions of the floe, the results presented are the x -directed and y -directed stress fields for only the top right quadrant of the floe. The forcing for each simulation was across a 600-m edge of the 3000-m-wide floe.

The results for the compressive forcing $\partial u/\partial x$ are shown in Figure 11. The results are scaled by the maximum stress in the x direction and then multiplied by 100. The stresses in the x direction show a maximum (100) near the outside edge of the floe at (1470 m, 0 m). Moving toward the center of the floe, the stresses decrease as shear within the floe redistributes the stresses in the y direction. All stresses are compressive (positive). For stresses in the y direction, maximum compressive stresses are seen to occur in the same region where maximum compressive, x -directed stresses are found; but these rapidly change to tensile stresses on moving toward the center of the floe, although they are relatively small (up to a relative value of -7). The two stress fields are symmetric relative to the central axes of the floe. These results are consistent with the stress distributions reported by Frederking and Evgin [1990] for the same loading conditions.

The results for the shearing force $\partial v/\partial x$ are shown in Figure 12. Again, the results are scaled to the maximum stress in the x direction and then multiplied by 100. As before, the stresses in the x direction show a maximum (100) near the outside edge of the floe at (1470 m, 0 m), with the stresses decreasing toward the center of the floe. Most stresses are compressive, but there is a region of tensile stresses along the upper right edge of the floe. The stresses in the y direction are an alternating pattern of compressive and tensile stresses, with maximum compressive stresses occurring in the same region where maximum compressive, x -directed stresses are found. The maximum tensile stresses are of the order of 50% of the maximum compressive stresses. There is a symmetry to these fields, but it is more complex than that of compressive forcing at the boundaries. The symmetry is such that the bottom left quadrant is identical to the top right quadrant. However, the top left and bottom right quadrants are mirror images of the top right quadrant, with compressive stresses being tensile and tensile stresses being compressive. As seen in Figure 12 (bottom), this results in an alternating pattern of eight regions of compression and eight regions of tension all around the floe for the conditions being modeled here.

5. Discussion of Analyses

Our study concentrates on understanding motion-induced stresses within typical floes in the Arctic. We have produced our best estimates of the motion-induced components of stress from stress gauge data collected at the main SIMI floe (Figure 7). These estimates are in terms of force per unit vertical area. We then applied a force balance argument and used wind, current, and ice motion data to calculate the net motion-induced stresses for the main SIMI floe (Figure 9). The calculated residual stresses are in terms of force per unit horizontal area. Of the three significant stress events determined by the force balance calculations, only the one event in the north-

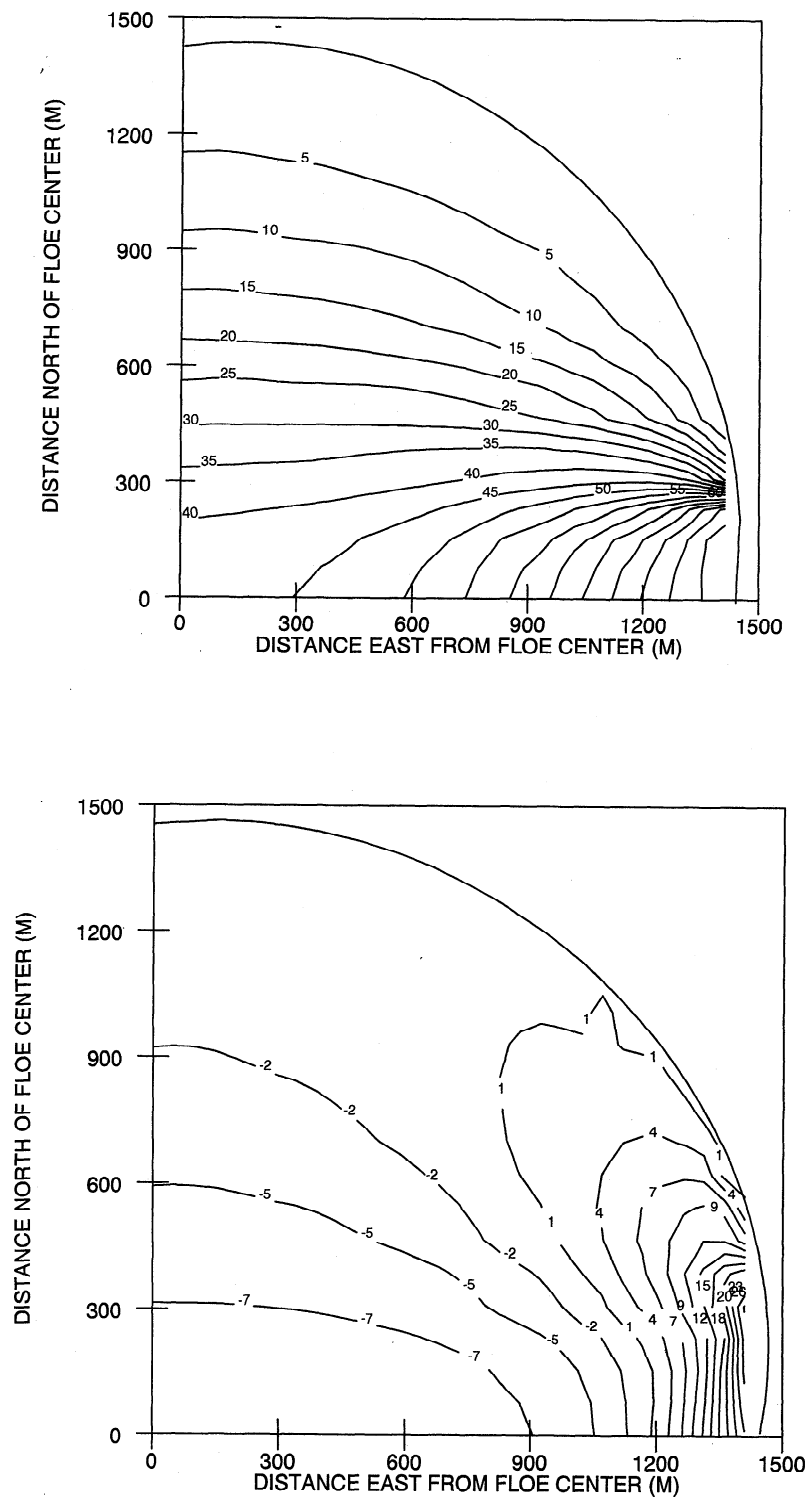


Figure 11. Relative compressive/tensile stresses in the (top) x direction and (bottom) y direction for the upper left quadrant of a nearly circular floe being forced with a strain rate $\partial u/\partial x = 10^{-6} \text{ s}^{-1}$.

south direction (days 356–359) had a strong corresponding signal in the stress gauge data. The strongest residual stress event was the east-west event during day 341, and there is very little indication of this stress event in the gauge data. The calculated residual stresses were then converted to force per unit vertical area and compared to the estimates of motion-induced stresses from the gauge data (Figure 10). To do this, we had to pick a horizontal width over which the residual

stresses were distributed. In the north-south direction, a width of 10 m produced a good reproduction of our estimates of the motion-induced stresses of σ_{yN} . In the east-west direction, the width chosen was 50 m. This larger width reduced the signature of the residual stress to the order of the variations of the motion-induced stresses seen in σ_{xE} . Together, these results suggest that in many instances we may have significant and dynamically important motion-induced stresses within a floe

the values of the ridge-building forces we use in models and those we actually observe from point stress measurements at ridge-building sites.

We can evaluate this discrepancy using the residual stress calculations shown in Figure 9. The calculations give us events with maximum magnitudes of ~ 0.4 Pa for an average ice thickness of 1.42 m. If we were working with an ice model with grid cells of the order of 100 to 125 km, a 0.4-Pa stress in terms of force per unit horizontal area would represent $\sim 28\text{--}35$ kPa of stress in terms of force per unit vertical area [e.g., $(0.4 \text{ Pa} \times 100 \text{ km} \times 100 \text{ km}) / (100 \text{ km} \times 1.42 \text{ m}) = 28.2 \text{ kPa}$]. This is approximately equal to the 25–30 kPa that is used in many Arctic sea ice models as the ridge-building force. However, this conversion of a 0.4 Pa maximum to 28–35 kPa ridge-building force assumes that the 0.4-Pa stress event is distributed over the entire length of the side of a model grid cell (100 km in the above example). As our analyses indicate, in reality, the distribution may be over a smaller length, which can increase the stress at a given site and might actually result in ridge building. For example, for an ice model with a grid with the same volume of the SIMI floe (3 km diameter, 1.42 m thick), a maximum magnitude of 0.4 Pa when distributed over the entire 3 km would convert to a ridge-building force of only 0.7 kPa in terms of force per unit vertical area [$(0.4 \text{ Pa} \times \pi \times 2.25 \text{ km}^2) / (2.659 \text{ km} \times 1.42 \text{ m}) = 0.7 \text{ kPa}$]. Yet the one event in S_y (Figure 9) has a corresponding signature in the gauge data of ~ 100 kPa (Figure 7). According to our analysis, this residual stress (order of 0.2 Pa) would be acting over a horizontal length of only ~ 10 m, not the larger horizontal scale of a grid with the same volume of the SIMI floe [that is, $(0.2 \text{ Pa} \times \pi \times 2.25 \text{ km}^2) / (10 \text{ m} \times 1.42 \text{ m}) = 100 \text{ kPa}$]. A force of 100 kPa conceivably could have resulted in some rafting or ridge building within the SIMI region, so if we were modeling the region with a grid with the same volume of the SIMI floe, we would have to set the ridge-building force to ~ 0.7 kPa. Thus the discrepancy between the magnitudes of actual ridge-building forces and a model ridge-building force is really just a matter of having to work with the scale of the grid in the model.

We now turn to the results of the numerical simulation of the distribution of motion-induced stresses within a floe. The principle result of these simulations is that the character of a motion-induced stress event is dependent not only on the area over which the stress is distributed but also the location in the floe at which observations are made. *Frederking and Evgin* [1990] had given some indication of the spatial distribution of stresses within a floe for compressive forcing, and we have repeated some of their simulations (Figure 11) using enhanced physics that include the creep of the ice and parameters that vary with strain rate, porosity, and temperature. We have also simulated motion-induced stresses as a result of shearing stress across the edges of a floe (Figure 12), a process not considered by *Frederking and Evgin* [1990]. Altogether, these simulations suggest the possibility that the seeming lack of a clear correspondence in the signature of the stress gauge data to the two major residual stress events in S_x may not be a result of the distribution of the force over a relatively large area. Instead, the lack of correspondence in the measured and calculated stress may simply be due to the difficulties of interpreting the local point measurements of stress in a system that exhibits significant horizontal spatial variability. As seen in Figure 12, if the stress event was caused by shearing stresses, the signature of the event could range from compression to practically zero

stress to tension, all depending on the location of the observations relative to the forcing.

These modeling results provide us with an enhanced interpretation of the scaling variables $\Delta x = 10$ m and $\Delta y = 50$ m when matching the residual stresses to the gauge stresses. In actuality, these represent a mean horizontal scale of force distribution based on the time-averaged location of the gauges relative to the forcing at the boundaries of the floe. We know that the locations of GN and GE relative to north and east varied with time (Figure 4), and the model results show us that changes in position relative to the central axis of forcing can result in different stress levels (Figures 11 and 12). For compressive forcing, a location nearer the center of the floe or farther from the axis of forcing will see smaller stress levels and thus will appear to have larger horizontal scales of distribution. The same is true for shear forcing, except there are locations at which the stress levels can get very small (passing from a region of positive to negative stress or visa versa) and thus the calculated scales of horizontal distribution could be quite large.

Although our study has provided us with a far better understanding and signatures of motion-induced stresses within a floe, we still lack the knowledge of how to relate the variations of our residual stress S with the differential motion as seen by the cluster of drifters (Figure 3). As our calculations have shown, the balance of forces can be approximated by $\tau_b - \tau_s = S$. Thus a formulation giving $S = f(\epsilon_{xx}, \epsilon_{xy}, \epsilon_{yy})$ would provide a key component for a dynamical model of the pack ice.

The differential motion for the study period is fairly simple, with the dominant strain rates being $\partial u / \partial x (\epsilon_{xx})$ and $\partial v / \partial x$ while the other strain rates, $\partial u / \partial y (\epsilon_{xy})$ and $\partial v / \partial y$, were negligible, for the most part. We have considered a number of plausible formulations relating S to these dominant strain rates, but we have been stymied by the fact that convergence of the ice pack ($\epsilon_{xx} < 0$) does not always correlate with increasing residual stresses (Figure 9). It can be shown that if $\partial v / \partial x$ is large enough, $\epsilon_{xx} < 0$ does not always lead to a decrease in distances between points of a grid covering a region of differential motion; but our calculations show that this situation did not occur during the study period, and $\epsilon_{xx} < 0$ should result in convergence of the floes. While the three main events seen in S all occurred while $\epsilon_{xx} < 0$, on the basis of the formulations we have tested so far, there also should have been some significant events during days 344–347 and 359–361.5 as a result of the substantial convergences of the ice pack during those times (Figure 9).

Obviously, the relationships between the residual stress in the ice pack and the differential motion of the floes need additional research and study. However, our results point out the possibility that the residual stresses might not be generated by local deformation of the ice. Perhaps the residual stress was transferred through the ice pack from a remote site, a process that can only occur when both (1) the ice has converged sufficiently across the pack to propagate the stress from a remote site and (2) there exists a stress at a remote site to propagate. This elastic transmission of stress is another factor to be considered in our continuing study of motion-induced stresses in pack ice.

6. Summary and Conclusions

Overall, the observations presented in this study add further confirming evidence that the process of stress transmission through the ice pack during periods of ice motion over scales of meters to tens of kilometers is extremely complex. We have

seen that some nonthermal events seen in the stress gauge observations could be related directly to the residual stresses determined from the balance of forces acting on the SIMI floe. However, other significant and dynamically important stress events were not discernible in the stress gauge observations. Our analyses indicate that the detection of stress events by a given stress gauge will be determined by (1) the location of the stress gauge relative to the location of the forcing on the floe and (2) the horizontal distance over which the stress event is distributed in the floe. Compressive forcing and, in particular, shearing forcing at the edge of a floe can result in complex patterns of stress throughout the floe, making the assessment of motion-induced stresses from individual gauge data a difficult task. Furthermore, we have found that there is not a logical formulation by which the stress events determined from the force balance equations can be related to the differential motion of the ice surrounding the SIMI floe. It is possible that, even for those motion-induced events that can be readily discerned from stress gauge observations, the forcing may be far field, not local. On the other hand, we must consider the possibility that the strain rates calculated using the surrounding ice drift data were not those actually acting along the edges of the SIMI floe. In other words, the strain data were not "local" enough, and we should have made direct observations of the interactions along the boundaries of the SIMI floe.

Developing our understanding of residual stresses within a floe will require combining (1) field measurements of ice stress, ice deformation, and wind and current forcing with (2) models of ice motion, the transmission of stress through the pack, and stress distribution within a floe. The apparent hierarchical nature of sea ice mechanics [Overland *et al.*, 1995] and the work being done on the motion of sand particles [Guterl, 1996] encourage us to recommend considering more carefully the role of the interactions of many floes within a given region (i.e., a granular approach to the modeling of the ice pack). Guterl [1996] describes a photoelastic experiment conducted by R. Behringer at Duke University to gain insight on the stress created by the interaction of circular particles. The article showed a stress pattern whose description is strikingly similar to the observations we have in this paper. The stress pattern exhibited significant spatial variability both within and between floes and showed dominant transmission paths that traveled through many connecting particles but totally bypassed many more particles in the same region. Thus, on the scales of 10–25 km, it is likely true that the granularity of the ice pack must be considered to fully comprehend floe movement, stresses within floes, and the transmission of stress through the pack. Fortunately, the ingredients already exist to conduct a study that would consider the granular nature of the ice pack. Hopkins [1996] demonstrated the application of a granular-based model to describe the mechanical behavior of the ice pack at the 10- to 100-km scale. This study and the work of Frederking and Evgin [1990] have shown the use of numerical simulations to describe stress distribution in individual floes. The stress and deformation data collected during SIMI provide the information necessary to evaluate the accuracy of the models. What remains is to put all of these ingredients together in a focused effort.

Acknowledgments. This work was supported by the Office of Naval Research through contracts to Scientific Solutions, Inc., and the Cold Regions Research and Engineering Laboratory. The GPS data used to determine relative ice motion and the wind velocity data were provided by J. Overland at NOAA's Pacific Marine Environmental Laboratory.

R. Pinkel at Scripps Institute of Oceanography, Marine Physical Laboratory, provided the ocean current data.

References

- Amorocho, J., and J. J. DeVries, Reply to "Comment on a new evaluation of the wind stress coefficient over water surfaces," *J. Geophys. Res.*, **86**, 4308, 1981.
- Cox, G. F. N., and J. B. Johnson, Stress measurements in ice, *Rep. 83-23*, Cold Reg. Res. and Eng. Lab., Hanover, N. H., 1983.
- Frederking, R. M. W., and E. Evgin, Analysis of stress distributions in an ice floe, paper presented at Ninth International Conference on Offshore Mechanics and Arctic Engineering, Am. Soc. of Mech. Eng., Houston, Tex., Feb. 18–23, 1990.
- Guterl, F., Riddles in the sand, *Discover*, 105–114, Nov. 1996.
- Hibler, W. D., III, A dynamic thermodynamic sea ice model, *J. Phys. Oceanogr.*, **9**, 815–846, 1979.
- Hopkins, M. A., On the mesoscale interaction of lead ice and floes, *J. Geophys. Res.*, **101**, 18,315–18,326, 1996.
- Johnson, J. B., and G. F. N. Cox, Stress sensor particularly suited for elastic, plastic, and viscoelastic materials, U.S. patent 4,346,600, Aug. 31, 1982.
- Kirwan, A. D., and M. S. Chang, Effects of sampling rate and random position error on analysis of drifter data, *J. Phys. Oceanogr.*, **9**, 382–387, 1979.
- Lewis, J. K., A model of thermally-induced stresses in multi-year sea ice, *Cold Reg. Sci. Technol.*, **21**, 337–348, 1994a.
- Lewis, J. K., Relating arctic ambient noise to thermally induced fracturing in the ice pack, *J. Acoust. Soc. Am.*, **95**, 1378–1385, 1994b.
- Lewis, J. K., Thermomechanics of pack ice, *J. Geophys. Res.*, this issue.
- Lewis, J. K., and M. R. Giuffrida, Sea-ice kinematics as determined by remotely-sensed ice drift: Seasonal space and time scales, *Photogramm. Eng. Remote Sens.*, **55**(8), 1113–1121, 1989.
- Mellor, M., Mechanical behavior of sea ice, in *The Geophysics of Sea Ice*, edited by N. Untersteiner, pp. 165–281, Plenum, New York, 1986.
- Overland, J. E., and C. H. Pease, Modeling the dynamics of coastal seas, *J. Geophys. Res.*, **93**, 15,619–15,637, 1988.
- Overland, J. E., B. A. Walter, T. B. Curtin, and P. Turet, Hierarchy and sea ice mechanics: A case study from the Beaufort Sea, *J. Geophys. Res.*, **100**, 4559–4571, 1995.
- Perovich, D. K., K. F. Jones, and W. B. Tucker III, Observations of stress in Arctic pack ice, paper presented at Eleventh Int. Symposium on Ice, Int. Assoc. of Hydraul. Res., Banff, Alberta, Canada, June 15–29, 1992.
- Perovich, D. K., B. C. Elder, and J. A. Richter-Menge, Observations of the annual cycle of sea ice temperature and mass balance, *Geophys. Res. Lett.*, **24**(5), 555–558, 1997.
- Preller, R. H., A. Cheng, and P. G. Posey, Preliminary testing of a sea ice model of the Greenland Sea, in *Proceedings of the W.F. Weeks Sea Ice Symposium, Monogr. 90-1*, pp. 259–277, Cold Reg. Res. and Eng. Lab., Hanover, N. H., 1990.
- Preller, R. H., J. E. Walsh, and J. A. Maslanik, 1992: The use of satellite observations in ice cover simulations, in *Microwave Remote Sensing of Sea Ice*, Geophys. Monogr. Ser., vol. 68, edited by F. D. Carsey, chap. 22, pp. 385–404, AGU, Washington, D. C., 1992.
- Pritchard, R. S., Mathematical characteristics of sea ice dynamics models, *J. Geophys. Res.*, **93**, 15,609–15,618, 1988.
- Richter-Menge, J. A., and B. C. Elder, Characteristics of pack ice stress in the Alaskan Beaufort Sea, *J. Geophys. Res.*, this issue.
- Richter-Menge, J. A., B. C. Elder, J. E. Overland, and S. Salo, Relating Arctic pack ice stress and strain at the 10 km scale, in *Proceedings of the ACSYS Conference on the Dynamics of the Arctic Climate System*, edited by P. Lemke, et al., *WMO/ITD Publ. 760*, pp. 327–331, World Meteorol. Organ., Geneva, 1996.
- Tucker, W. B., III, Applications of a numerical sea ice model to the East Greenland area, *Rep. 82-16*, 40 pp., Cold Reg. Res. and Eng. Lab., Hanover, N. H., 1982.
- J. K. Lewis, Ocean Physics Research & Development, 207 South Seashore Avenue, Long Beach, MS 39560. (e-mail: ocnphys@aol.com)
- J. A. Richter-Menge, Cold Regions Research and Engineering Laboratory, Hanover, NH 03755.

(Received April 21, 1997; revised January 12, 1998; accepted January 23, 1998.)